Süleyman Demirel Üniversitesi Fen Edebiyat Fakültesi Fen Dergisi
Süleyman Demirel University Faculty of Arts and Sciences Journal of Science
2019, 14(2): 285–295
DOI: 10.29233/sdufeffd.549528
Atıf için / For Citation: T. MERCAN, G. SEVİM, Y. A. ÜNCÜ, S. USLU, H. Ö. KAZANCI, M. CANPOLAT, "The comparison of reconstruction algorithms for diffuse optical tomography", *Süleyman Demirel Üniversitesi Fen Edebiyat Fakültesi Fen Dergisi*, 14(2), 285–295, 2019.

The Comparison of Reconstruction Algorithms for Diffuse Optical Tomography

Tanju MERCAN[1], Gençay SEVİM[1], Yiğit Ali ÜNCÜ[1], Serkan USLU[1], Hüseyin Özgür KAZANCI[2], Murat CANPOLAT[*1]

[1]*Akdeniz University, School of Medicine, Department of Biophysics, 07058, Antalya, Turkey*
[2]*Akdeniz University, Faculty of Engineering, Department of Biomedical Engineering, 07058, Antalya, Turkey*

**Corresponding author e-mail: canpolat@akdeniz.edu.tr*

(Alınış / Received: 05.04.2019, Kabul / Accepted: 23.09.2019, Yayımlanma / Published: 30.11.2019)

Abstract: Diffuse optical tomography (DOT) utilizes wavelength range of 750-950 nm to map the spatial distribution of the tissue chromophores of breast tissue for cancer diagnosis or follow up prognosis. DOT allows tomographic reconstructions of tissue optical properties. Several reconstruction methods have been developed to minimize artifacts and obtain more realistic tomographic images. In order to compare four different reconstruction algorithms, data acquired from tissue phantoms using a DOT system. Algebraic reconstruction technique (ART), simultaneous iteration reconstruction technique (SIRT), truncated singular value decomposition (TSVD) and truncated conjugate gradient (TCG) techniques have been compared in terms of location of inclusion in the tissue phantoms. It has been shown that images reconstructed by the subspace techniques, TSVD and TCG locating the inclusion position better than the algebraic methods ART and SIRT. Beside, images reconstructed by TSVD and TCG have less artifact when compared to images of ART and SIRT.

***Key words**:* Algebraic reconstruction technique, Simultaneous iteration reconstruction technique, Truncated singular value decomposition, Truncated conjugate gradient, Diffuse optical tomography

Diffüz Optik Tomografi için Yeniden Yapılanma Algoritmalarının Karşılaştırılması

Özet: Diffüz optik tomografi (DOT), kanser tanısı veya kanser takibi için meme dokusunun doku kromoforlarının uzaysal dağılımını görüntülemek için 750-950 nm dalga boyu aralığını kullanır. DOT, doku optik özelliklerinin geri çatım teknikleri ile tomografik olarak gösterilmesini sağlar. Görüntülerdeki gürültüleri en aza indirmek ve daha gerçekçi tomografik görüntüler elde etmek için çeşitli geri çatım teknikleri geliştirilmiştir. Dört farklı geri çatım tekniklerini karşılaştırmak için DOT sistemi ile doku fantomu kullanılarak veriler elde edildi. Doku fantomundaki inklüzyonun konumu belirleme açısından Cebirsel geri çatım tekniği (ART), eşzamanlı cebirsel geri çatım tekniği (SIRT), tekil nokta ayrışması (TSVD) ve kesikli eşlenik gradyent (TCG) teknikleri karşılaştırılmıştır. Alt uzay tekniklerinden TSVD ve TCG ile oluşturulan görüntülerdeki inklüzyonun konumu, cebirsel yöntemlerden ART ve SIRT' den daha iyi konumlandırıldığı gösterilmiştir. Ayrıca, TSVD ve TCG tarafından oluşturulan görüntüler, ART ve SIRT ile oluşturulan görüntülere göre daha az gürültü olarak elde edilmiştir.

Anahtar kelimeler: Cebirsel geri çatım tekniği, Eşzamanlı cebirsel geri çatım tekniği, Tekil nokta ayrışması, Kesikli eşlenik gradyent, Diffüz optik tomografi

Tanju MERCAN, tanjumercan@akdeniz.edu.tr, ORCID: https://orcid.org/0000-0002-6711-6003
Gençay SEVİM, gncy.svm@gmail.com, ORCID: https://orcid.org/0000-0002-2157-3209
Yiğit Ali ÜNCÜ, yuncu@akdeniz.edu.tr, ORCID: https://orcid.org/0000-0001-7398-9540
Serkan USLU, serkanuslu@akdeniz.edu.tr, ORCID: https://orcid.org/0000-0002-0875-5905
H. Özgür KAZANCI, ozgurkazanci@akdeniz.edu.tr, ORCID: https://orcid.org/0000-0003-0036-7657
Murat CANPOLAT, canpolat@akdeniz.edu.tr, ORCID: https://orcid.org/0000-0003-3298-9725

1. Introduction

Over the past two decades, diffuse optical tomography (DOT) techniques have been developed to estimate optical properties of interior tissue for diagnostic proposes [1-6]. Near-infrared (NIR) light in the range of 750-900 nm, named as body window, has been used in DOT systems. Data in the DOT system were acquired in transmission or back reflection geometry [7]. Monte Carlo (MC) simulation results of DOT systems were also used to reconstruct object with similar optical properties to breast or brain tissues [8-10]. Results of the MC simulation may be noise free, or an amount of the noise may be added artificially as desired. Therefore, MC simulation has been used as a powerful tool to tests the reconstruction algorithms.

Several groups have developed different reconstruction methods based on non-linear and back-propagation techniques [10-12]. Nonlinear models are computationally very expensive due to minimizing the number of assumptions regarding tissue optical properties. Back-propagation is computationally economical but have a poor spatial resolution in separating multiple absorbing objects [13, 14]. Linear methods of the forward model established by Born or Rytov approximations and have been explored by others [15-17]. Weight matrix in the linear model was obtained using Monte Carlo (MC) simulations for a homogeneous medium with similar optical properties of the tissues [8, 18, 19].

Previously, David Boas et al. published a comparison study of linear reconstruction techniques using MC simulations results [20]. Two class linear reconstruction techniques, algebraic and subspace methods were compared in simple back-reflection geometry. The ART and SIRT have been described [17] as algebraic techniques. The TSVD [21] and TCG algorithms have been described as subspace techniques [22, 23].

In the presented work, a diffuse reflection DOT system has been used to acquire data from breast tissue phantoms consist of Intralipid and Indocyanine green (ICG). In this paper, this is the first time we compare four algorithms which data are taken from tissue phantom. The tissue phantoms have been reconstructed using linear reconstruction techniques ART, SIRT, TCG, and TSVD and compared to each other in terms of artifacts and defining the correct location of the inclusions.

2. Material and Method

2.1 System design

The DOT system consists of a continuous wave (CW) diode laser with wavelength of 808 nm, a 1x49 optical switch, an optical fiber imaging probe with sources and detector fibers, a PC. The system electronics are composed of photodiodes and electronic boards [24]. Schematic representation of the system is shown in Figure 1. The optical switch directs the light to 49 optical fibers of the optical probe sequentially for a defined period. Diffuse back-reflected light from the tissue phantom is received by 49 optical fibers and delivered to the photodiodes. All source and detector fibers diameter are 1 mm in Figure 2. The probe has a total of 22 different source-detector pair, so the light penetrates 22 different depths.

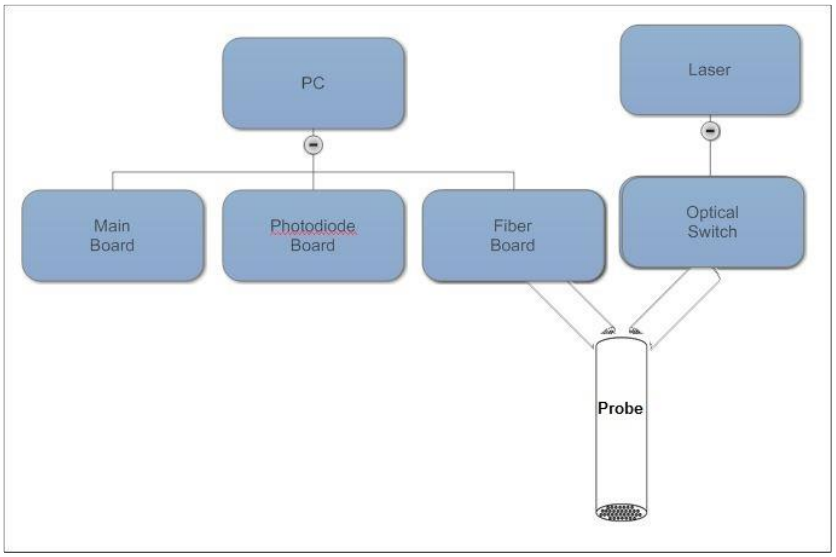

Figure 1. Schematic representation of the system. The optical switch directs the laser to the fiber of the probe used as sources. The back reflected light is received by the detector fibers of the probe and send to the photodiodes. Digitized data is transferred to the PC.

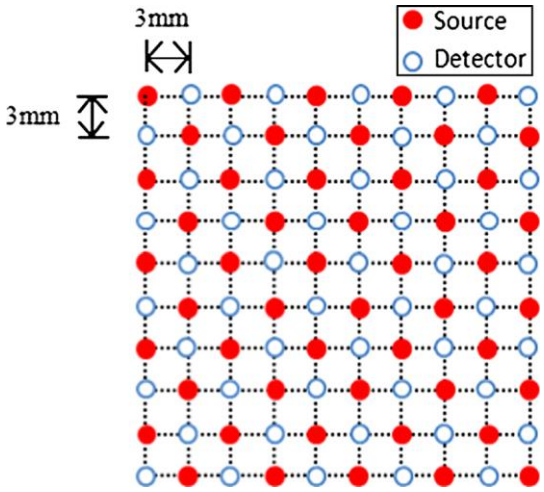

Figure 2. Surface of the probe. All of the optical fibers with a core diameter of 1 mm located on a 10x10 square matrix. Two of the matrix location is empty. There are 98 fibers on the probe surface.

2.2 Tissue phantom experiments

Tissue phantom was a mixture of 1% Intralipid solution and ICG with reduced scattering coefficient *(μs')* and absorption *(μa)* coefficients of 10 cm^{-1} and 0.04 cm^{-1}. A black rectangular container with dimensions 25 cm x 25 cm x 15 cm was filled with the mixture in order to prevent penetration of ambient light in the tissue phantom and back reflection of the laser light from the container. The probe was placed on the surface of the Intralipid and first measurement, M_{hom}, was acquired from the homogenous phantom with 2401 (49x49) data points, where for each source position the back reflected light received by the all 49 optical fibers used as detectors. Then, a spherical inclusion was prepared by filling a transparent balloon with 1% Intralipid solution and ICG with $\mu s'$=10 cm-1 and μa=0.16 cm^{-1} respectively. Absorption contrast is four times higher than the background. The diameter of the inclusion was 0.8 cm and placed depths of 0.7 cm and 1.2 cm from the center of the inclusions of the tissue phantom and measurements, M_{mes}, were acquired. Measurement from the homogenous phantom M_{hom} is used for the calibration proposes [24]. The calibrated data is $R = M_{mes}/M_{hom}$.

2.3 The forward model for diffuse optical imaging

The photon fluence rate *Ø(r,t)*(photons/(cm^2.s)) obeys the following diffusion approximation to the radiative transport equation in scattering medium [25].

$$D\nabla^2\emptyset(r) - v\mu_a\,(r)\emptyset(r) = -vS(r) \tag{1}$$

where *v* is the speed of light in the material, *S(r)* is the anisotropic photon source and *D* is diffusion constant

$$D = \left[3\left(\mu_a + \mu'_s\right)\right]^{-1}. \tag{2}$$

In order to solve Equation 1 Rytov approximation is used [15, 26], where the total fluence defined as

$$\emptyset(\mathrm{r}) = \emptyset_0(\mathrm{r})\exp[\emptyset_{\mathrm{sc}}(\mathrm{r})] \tag{3}$$

where $\emptyset_0$ is the homogenous part of the fluence rate and $\emptyset_{sc}$ is the perturbed fluence induced by the inclusion [3]. Substituting Equation 3 in Equation 1 gives a linear solution of

$$y = Ax \tag{4}$$

Where *y* is a 1D array with a dimension of *m* of the perturbation data. *A* is the weight matrix obtained from MC simulation with a dimension of *m* × *n*, where *m*, the number of the data in each acquisition and *n*, the number of the voxels. *x* is the in the absorption perturbation vector with a dimension of *n*. The weight matrix was obtained using MC simulations which have been described previously [24].

2.4 Reconstruction techniques

Generally, reconstruction techniques used in DOT systems are ART, SIRT [17], TSVD [23], and TCG [27]. Usually, reconstruction techniques are categorized into two groups, algebraic techniques, and subspace techniques. Two of the most popular algebraic techniques are ART and SIRT. ART reconstruct an image from a series of angular projections. The projection starts with an initial guess, which is usually zero. After each iteration, the previous solution is used as an initial value, and every projection sequentially approaches into hyper planes. Below projection is used to estimate the solution for the next iterations.

$$x_{j+1} = x_j + w\frac{y_i - a_i x_j}{a_i a_i^T}a_i^T \qquad j = 0,1,\ldots \qquad i = (j\ mod\ m) + 1 \tag{5}$$

Where x_j is the j^{th} estimate of the unknown objects, a_i is the i^{th} row of the *m x n* matrix *A*, and y_i is the i^{th} measurement. *w* is a relaxation parameter which sets the step size for each iteration. Each iteration runs over one measured perturbation data and over all voxels parameter. If the iteration number is small, the relaxation parameter should be chosen close to 1. SIRT algorithm is different from the ART, each iteration run over all measured perturbation data to update the voxels unknown parameter, such as absorption coefficient. Though SIRT takes more time than ART, converges is much slower than ART and gives better images [17]. Mathematically this can be written as

$$x_{j+1} = x_j + w\frac{1}{m}\sum_{i=1}^{m}\frac{y_i - a_i x_j}{a_i a_i^T}a_i^{\mathrm{T}}. \quad (6)$$

Two of the subspace techniques are TSVD and TCG techniques. The TSVD algorithm is derived from the singular value decomposition (SVD) of the $N_{mes} \times N_{vox}$ weight matrix *A*. This theorem states [21]:

$$A_{mxn} = U_{m\times m}\, S_{m\times n}\, V^T_{n\times n} \quad (7)$$

Where, the columns of *U* are the left singular vectors; *S* has singular values and is diagonal, and V^T has rows that are the right singular vectors. It represents an expansion of the original data in a coordinate system where the covariance matrix is diagonal. The calculation of SVD consists of finding the eigenvalue and eigenvectors of AA^T and A^TA. The singular values are the diagonal entries of the *S* matrix and are arranged in descending order. The singular values are real numbers. If the matrix *A* is a real matrix, then *U* and *V* are real.

$$\sigma_1 \geq \sigma_2 \geq \cdots \geq \sigma_r \quad (8)$$

Where σ_i is the singular value of A and *r* is the rank of A. TSVD algorithm uses the largest *t* non-zero singular values and singular vectors. This is formulated as

$$x = V_t S_t^{-1} U_t^T\, y \quad (9)$$

Where V_t and U_t are the first *t* columns of *V* and *U* respectively, S_t^{-1} is the inverse of the square diagonal sub matrix of the largest *t* singular values. The value *t* is the truncation parameter which controls the degree of the solution. It has been provided in the literature about the SVD and TSVD [22, 28].

The TCG method for the numerical solution of linear equations given, so that the matrix is an algorithm for symmetric and positive definite. It is an iterative technique that has been used to solve a symmetric positive definite linear system. For ill condition problems, converging is a challenging issue so that iterations could be stopped [22]. The iteration number determines the degree of the solution. It technique can be applied to the normal equations given by

$$A^TAx = A^Ty. \quad (10)$$

A matrix is obtained using a Monte Carlo simulation of the light transport for the same source-detector distances as the optical probe. Obtaining the *A* is described in detail elsewhere [24]. Reconstruction was performed with a uniform mesh of 2250 voxels.

3. Results

All the measurements were acquired from the tissue phantoms without and with an inclusion. The volume of the region of interest in the Intralipid tank was 3.9cm × 3.9cm × 2.4cm and the number of the voxels is 15 × 15 × 10. So, the dimension of a voxel is 2.6 × 2.6 × 2.4 mm. After the calibration of the data, the reconstruction techniques were used to reconstruct the tissue phantoms with the inclusions at a depth of 0.7 cm and 1.2 cm from the center of the inclusions.

All the reconstruction techniques find the inclusion roughly in true position for the depth of 0.7 cm as seen in Figure 3. However, artifacts of the images are different for each reconstruction technique as seen in the x-z plane.

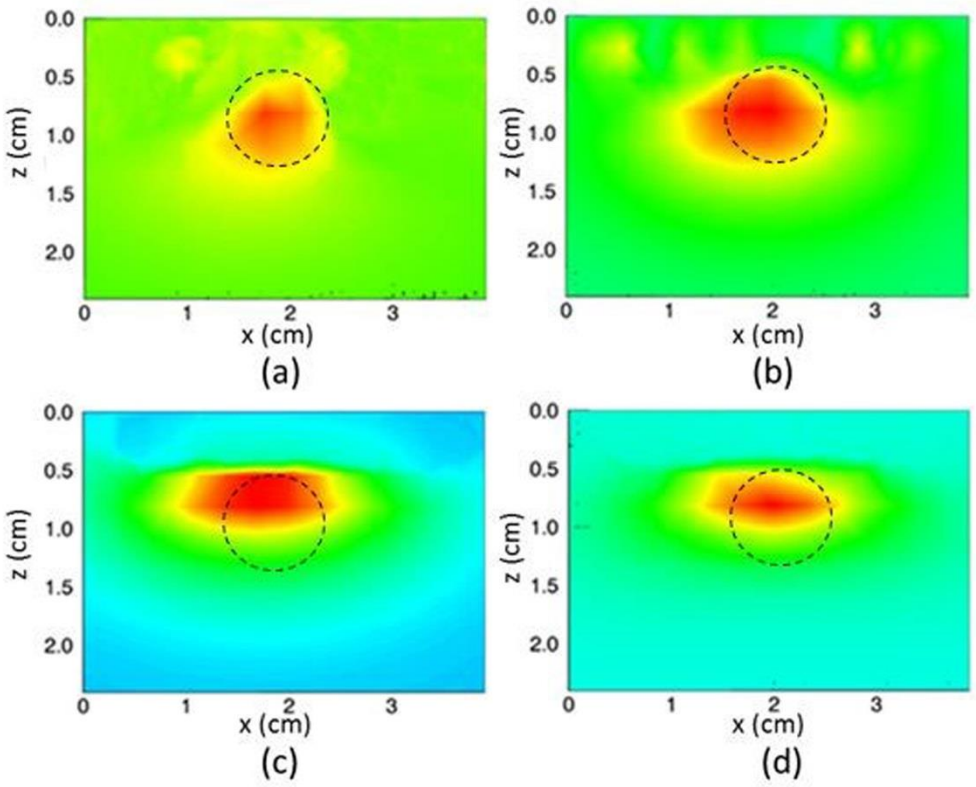

Figure 3. Reconstructed the tissue phantom with inclusion at a depth of 0.7 cm with the reconstruction techniques of (a) ART with 10 iterations. (b) SIRT with the 70 iterations. (c) TSVD with 100 singular values, (d) TCG with three iterations. All the images show the x-z plane.

Figure 3a is reconstructed by ART using 10 iterations, where there are lots of artifacts, and the location is not accurate, roughly center of the inclusion 3 mm deeper than the actual depth. Figure 3b is obtained using SIRT with 70 iterations. SIRT gives more accurate location and shape of the inclusion closer to actual one than ART. Figure 3c displays the reconstructed image by the TSVD algorithm employing 100 singular values. For this image, 100 singular values are optimum value because under the 100 singular values we cannot reconstruct a meaningful image and over 100 singular values artifacts are observed. Center of the inclusion is close to the actual location. Figure 3d shows the reconstructed image by TCG algorithm with three iterations.

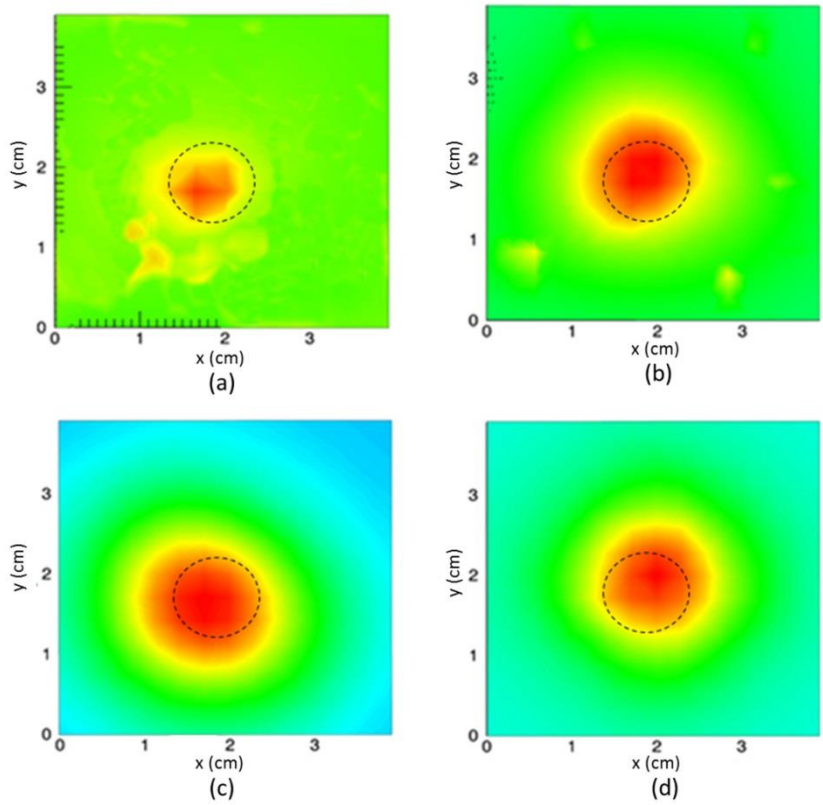

Figure 4. Reconstructed images are presented in the x-y plane. (a) ART algorithm with 10 iterations. (b) SIRT algorithm with the 70 iterations. (c) TSVD algorithm with 100 singular values. (d) TCG algorithm with three iterations.

Reconstructed images in Figure 3 are presented in the x-y plane in Figure 4 for the inclusion with the location coordinates of x=2 cm, y=2 cm and z=0.7 cm. As seen in Figure 4c and 4d, reconstructed image by TSVD and TCG are artifact free. However, the center of the inclusion position is shifted to the left in Figure 4c. TCG algorithm gives a better location in Figure 4d.

Reconstructed images of the tissue phantom with the inclusion at a depth of 1.2 cm from the center of the inclusion are shown in Figure 5. The shape of the inclusion's image has been changed in the x-z plane. It doesn't look like a sphere. It has been suppressed up and down.

Figure 5a is the reconstruction image using six iterations of ART. Figure 5b is the reconstruction image using 15 iterations of SIRT. ART and SIRT have very similar reconstructed images. Figure 5c displays the reconstruction for the TSVD algorithm employing 408 singular values. Figure 5d shows the reconstruction for the TCG algorithm with 30 iterations.

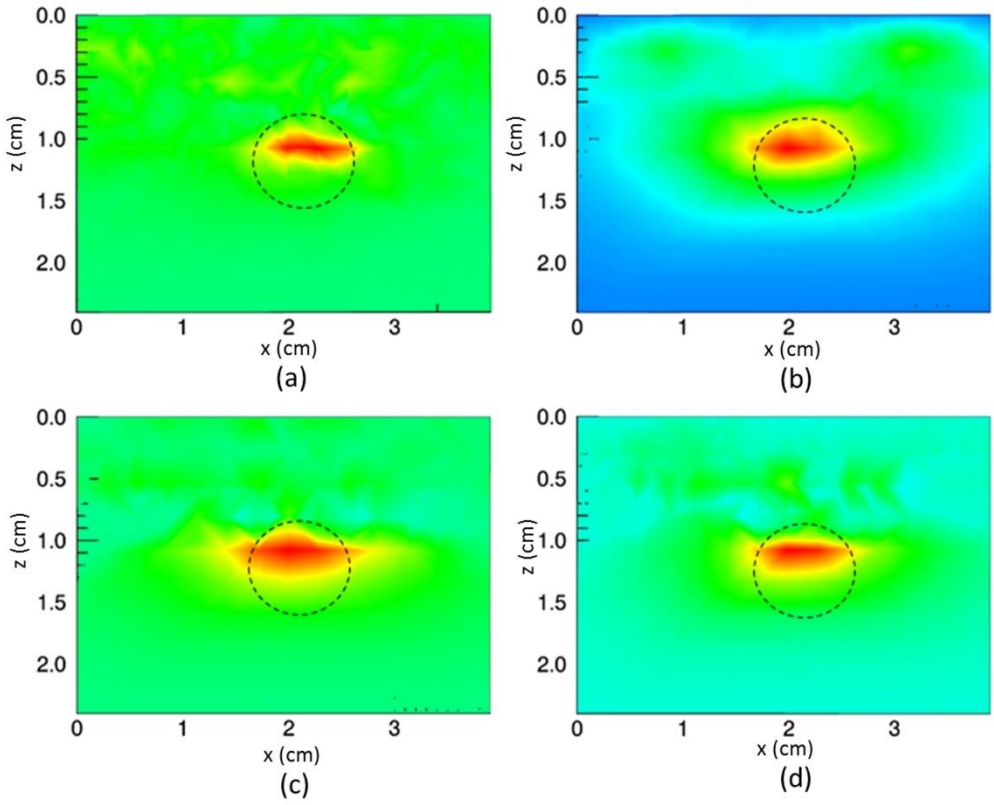

Figure 5. Reconstructed tissue phantom with inclusion at a depth of 12 mm. All the images in the x-z plane. Reconstruction performed by (a) ART algorithm with six iterations. (b) SIRT algorithm with the 15 iterations. (c) TSVD algorithm with 408 singular values. (d) TCG algorithm with 30 iterations.

Reconstructed images are presented in the x-y plane for the inclusion with the location coordinates of x=2 cm, y=2 cm and z=1.2 cm in Figure 6. As seen in Figures 6c and 6d, reconstructed image by TSVD and TCG are artifact free. Nevertheless, in Figure 6c the shape of the reconstructed image is bigger than the inclusions. Therefore, TCG algorithm has superiority over all other algorithms in estimating the location of the inclusion without artifacts.

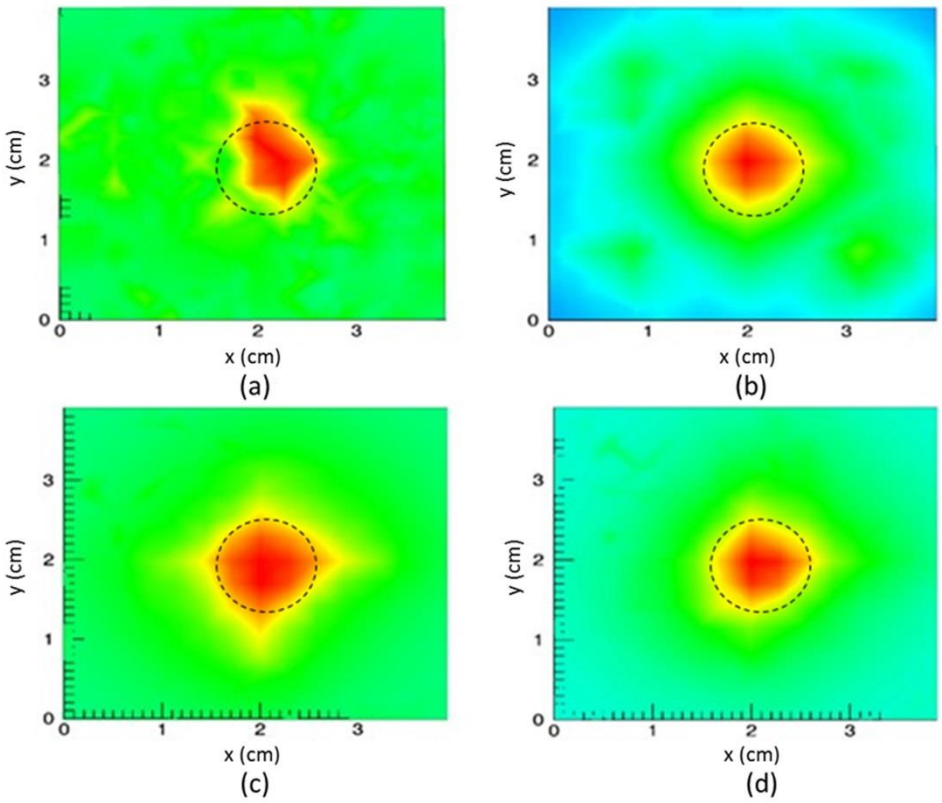

Figure 6. Reconstructed images in Figure 5 are presented in x-y plane, images are reconstructed by (a) ART algorithm with 6 iterations. (b) SIRT algorithm with the 15 iterations. (c) TSVD algorithm with 408 singular values. (d) TCG algorithm with 30 iterations.

4. Conclusion and Comment

The main purpose of this study was to investigate which reconstruction algorithm gives a better result. Boas, D.A., *et al.* showed that subspace techniques were superior to algebraic techniques from under-determined systems using results of MC simulations. Our system also shows that subspace techniques are superior to algebraic techniques. Since our system is over determined, algebraic techniques do not have a unique solution. Therefore, images reconstructed by ART and SIRT have more artifacts. Boas *et al*., find the iteration numbers of TCG and singular values of TSVD by using L-curve. However, for ART and SIRT they choose the iteration numbers of the best image manually [20]. Since our system is over determined L-curve did not work to obtain the iteration number of the best image. Therefore, we manually defined the iteration numbers for all reconstruction algorithms.

In this study, we know the location and shape of the inclusion, so we choose singular values and iteration numbers accordingly. For TCG, ART, and SIRT, the iteration number is selected by images created with different iteration numbers. These iteration numbers start from 1 and increase step by step. After a certain iteration number, the images started to blur. For each technique, we compared images and choose the best-reconstructed one. We followed the same path for TSVD to find the best singular value.

In our system, the matrix **A** is non-singular, so the images give less noisy and correct location of the inclusion [29]. For algebraic reconstruction techniques, if there are more equations than unknowns, then no unique solution exists, and the final solution

oscillates in the neighborhood of the correct solution. In our system, we have 2401 equations and 2250 unknowns. SIRT gives less noisy images than ART because for one iteration ART update unknowns over one equation, SIRT algorithm updates the unknowns through all the equations. Therefore, at the expense of slower convergence, usually, SIRT leads to better images than those produced by ART.

In this paper, we have compared reconstructed images of four linear reconstruction methods using the data acquired from the tissue phantoms by the back-reflection DOT system the first time. The images were obtained by linear reconstruction and the best image was obtained by the TCG algorithm. In our best knowledge, this is the first study that used data of a DOT system to compare the linear reconstruction techniques. One of the biggest drawbacks is of the presented study is defining the iteration number manually for all reconstruction methods. The iteration number may change from one DOT system to the other one. However, the presented study gives a rough idea about the iteration number for the four linear reconstruction algorithms in order to obtain the best image. We are currently working on development an automatic method to define the iteration number.

References

[1] A. Yodh and B. Chance, "Spectroscopy and imaging with diffusing light," *Physics Today*, 48, 34-40, 1995.

[2] H. B. Jiang, N. V. Iftimia, Y. Xu, J. A. Eggert, L. L. Fajardo, and K. L. Klove, "Near-infrared optical imaging of the breast with model-based reconstruction," *Academic Radiology*, 9, 186-194, 2002.

[3] Z. Yuan, Q. Z. Zhang, E. S. Sobel, and H. B. Jiang, "Image-guided optical spectroscopy in diagnosis of osteoarthritis: a clinical study," *Biomedical Optics Express*, 1, 74-86, 2010.

[4] Z. Yuan, "Combining independent component analysis and Granger causality to investigate brain network dynamics with fNIRS measurements," *Biomedical Optics Express*, 4, 2629-2643, 2013.

[5] R. C. Mesquita, M. A. Franceschini, and D. A. Boas, "Resting state functional connectivity of the whole head with near-infrared spectroscopy," *Biomedical Optics Express*, 1, 324-336, 2010.

[6] D. Lighter, J. Hughes, I. Styles, A. Filer, and H. Dehghani, "Multispectral, non-contact diffuse optical tomography of healthy human finger joints," *Biomedical Optics Express*, 9, 1445-1460, 2018.

[7] V. Ntziachristos, "Fluorescence molecular imaging," *Annual Review of Biomedical Engineering*, 8, 1-33, 2006.

[8] L. Wang, S. L. Jacques, and L. Zheng, "MCML—Monte Carlo modeling of light transport in multi-layered tissues," *Computer Methods and Programs in Biomedicine*, 47, 131-146, 1995.

[9] B. J. Tromberg, Z. Zhang, A. Leproux, T. D. O'Sullivan, A. E. Cerussi, P. M. Carpenter, *et al.*, "Predicting Responses to Neoadjuvant Chemotherapy in Breast Cancer: ACRIN 6691 Trial of Diffuse Optical Spectroscopic Imaging," *Cancer Research*, 76, 5933-5944, 2016.

[10] T. Shimokawa, T. Ishii, Y. Takahashi, S. Sugawara, M.-a. Sato, and O. Yamashita, "Diffuse optical tomography using multi-directional sources and detectors," *Biomedical Optics Express*, 7, 2623-2640, 2016.

[11] S. R. Arridge and M. Schweiger, "A gradient-based optimisation scheme for optical tomography," *Optics Express*, 2, 213-226, 1998.

[12] S. R. Arridge and M. Schweiger, "Image reconstruction in optical tomography," *Philosophical Transactions of the Royal Society of London B: Biological Sciences*, 352, 717-726, 1997.

[13] C. L. Matson, N. Clark, L. McMackin, and J. S. Fender, "Three-dimensional tumor localization in thick tissue with the use of diffuse photon-density waves," *Applied Optics*, 36, 214-220, 1997.

[14] S. B. Colak, D. G. Papaioannou, G. W. tHooft, M. B. vanderMark, H. Schomberg, J. C. J. Paasschens, *et al.*, "Tomographic image reconstruction from optical projections in light-diffusing media," *Applied Optics*, 36, 180-213, 1997.

[15] T. Durduran, R. Choe, W. B. Baker, and A. G. Yodh, "Diffuse optics for tissue monitoring and tomography," *Reports on Progress in Physics*, 73, 2010.

[16] R. Endoh, A. Suzuki, M. Fujii, and K. Nakayama, "Fundamental study on diffuse reflective optical tomography," *Physics in Medicine and Biology*, 49, 1881, 2004.

[17] A. C. Kak and M. Slaney, *Principles of computerized tomographic imaging*: SIAM, 2001.

[18] S. L. Jacques and L. Wang, "Monte Carlo modeling of light transport in tissues," in *Optical-Thermal response of laser-irradiated tissue*, ed: Springer, 1995, pp. 73-100.
[19] D. A. Boas, J. P. Culver, J. J. Stott, and A. K. Dunn, "Three dimensional Monte Carlo code for photon migration through complex heterogeneous media including the adult human head," *Optics Express*, 10, 159-170, 2002.
[20] R. J. Gaudette, D. H. Brooks, C. A. DiMarzio, M. E. Kilmer, E. L. Miller, T. Gaudette, *et al.*, "A comparison study of linear reconstruction techniques for diffuse optical tomographic imaging of absorption coefficient," *Physics in Medicine & Biology*, 45, 1051, 2000.
[21] W. H. Press, B. P. Flannery, S. A. Teukolsky, and W. T. Vetterling, *Numerical recipes in C: the art of scientific computing*: Cambridge University Press, 1988.
[22] P. C. Hansen, *Rank-Deficient and Discrete Ill-Posed Problems*: SIAM, 1998.
[23] O. Alter, P. O. Brown, and D. Botstein, "Singular value decomposition for genome-wide expression data processing and modeling," *Proceedings of the National Academy of Sciences of the United States of America*, 97, 10101-10106, 2000.
[24] H. O. Kazanci, T. Mercan, and M. Canpolat, "Design and evaluation of a reflectance diffuse optical tomography system," *Optical and Quantum Electronics*, 47, 257-265, 2015.
[25] T. J. Farrell, M. S. Patterson, and B. Wilson, "A Diffusion-Theory Model of Spatially Resolved, Steady-State Diffuse Reflectance for the Noninvasive Determination of Tissue Optical-Properties Invivo," *Medical Physics*, 19, 879-888, 1992.
[26] S. R. Arridge, "Optical tomography in medical imaging," *Inverse Problems*, 15, R41-R93, 1999.
[27] R. J. Gaudette, D. H. Brooks, C. A. DiMarzio, M. E. Kilmer, E. L. Miller, T. Gaudette, *et al.*, "A comparison study of linear reconstruction techniques for diffuse optical tomographic imaging of absorption coefficient," *Physics in Medicine and Biology*, 45, 1051-1070, 2000.
[28] G. H. Golub and C. F. V. Loan, *Matrix computations (3rd ed.)*: Johns Hopkins University Press, 1996.
[29] M. A. O'Leary, "Imaging with diffuse photon density waves," Physics, University of Pennsylvania; United States, 1996.